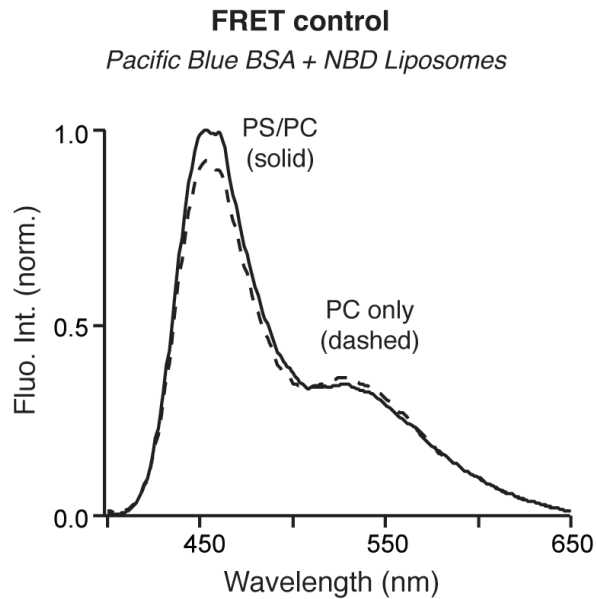


Supplemental Materials

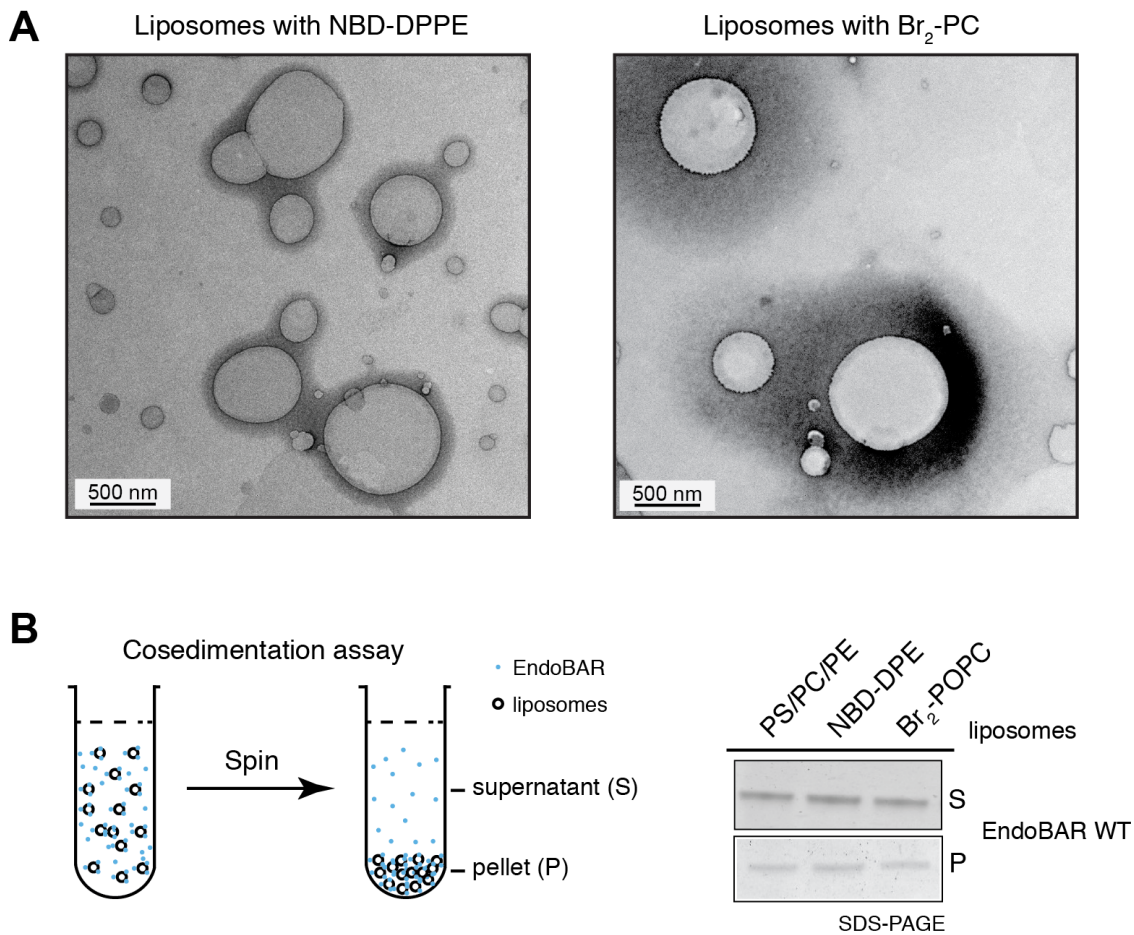
Molecular Biology of the Cell

Poudel et al.

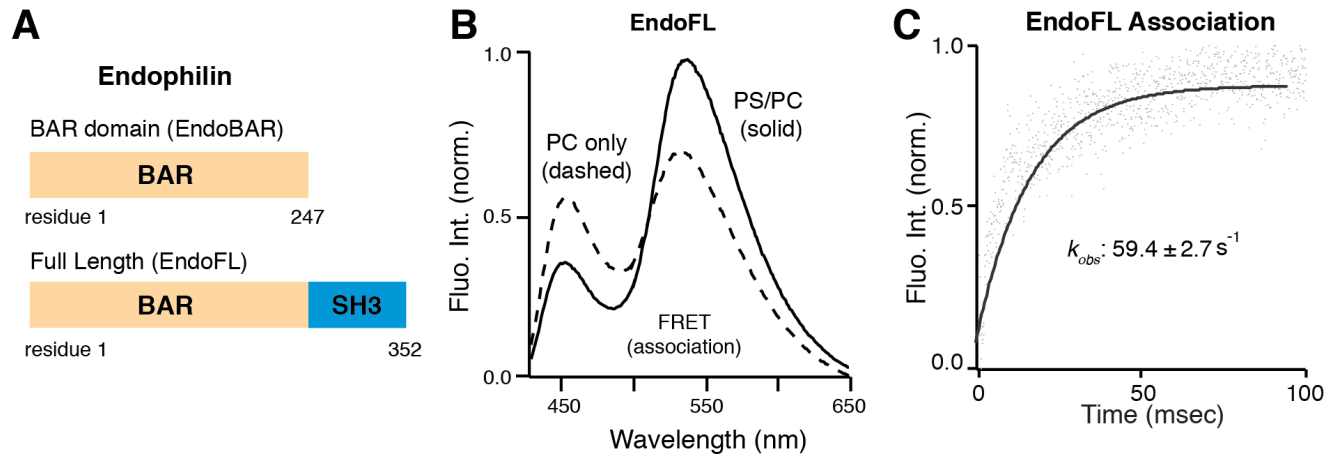


Supplementary Figure 1. Bovine Serum Albumin (BSA) does not induce FRET signals.

BSA was labeled with the donor fluorescent probe Pacific Blue (PB) as described in Methods. Emission spectra were collected as described in the legend of Figure 1. “PS/PC” indicates liposomes harboring 25%DOPS, 70%POPC, 5%NBD-DPPE; and “PC only” indicates liposomes that are composed of 95%POPC and 5%NBD-DPPE. Because BSA has 36 native cysteine residues, more PB fluorophores are labeled onto each BSA molecule. As a result, BSA-PB complexes show much higher donor fluorescence at 460 nm than EndoBAR-PB (Figure 1B). Incubation of BSA-PB (1 μ M BSA) with PS/PC liposomes (0.5 mM total lipids; ‘1 μ m filter’) slightly quenched NBD-PE fluorescence, suggesting that FRET signal (shown in Figure 1B) is not due to non-specific protein-membrane interactions. Experiments were repeated in three independent trials.



Supplementary Figure 2. Fluorescent reporters and membrane-embedded quenchers do not alter liposome property and EndoBAR-membrane association. (A) Negative staining electron microscopy images of NBD-PE liposomes (25%DOPS, 70%POPC, and 5%NBD-DPPE) and Br₂-PC (25%DOPS, 70%(9,10)-Br₂-PC, and 5%DPPE) are shown in panel A. (B) Cosedimentation experiments were used to analyze EndoBAR-membrane interactions. A schematic diagram of the cosedimentation assay is shown in *left panels*. Results from SDS-PAGE gels (*right panels*) show that NBD-DPPE and Br₂-PC do not alter EndoBAR-membrane interactions. “Blank” indicates liposomes that are composed of 25%DOPS, 70%POPC, and 5%DPPE. All experiments were repeated in three independent trials.



Supplementary Figure 3. Full length endophilin exhibits similar kinetic behavior of

membrane association as the isolated BAR domain. (A) A schematic diagram shows the

comparison between EndoBAR and the full length endophilin (EndoFL). (B-C) The steady-state

emission spectra and the stopped-flow kinetic trace from the FRET assays detected EndoFL-

membrane interactions experiments were carried out as described in the legend of Figure 1,

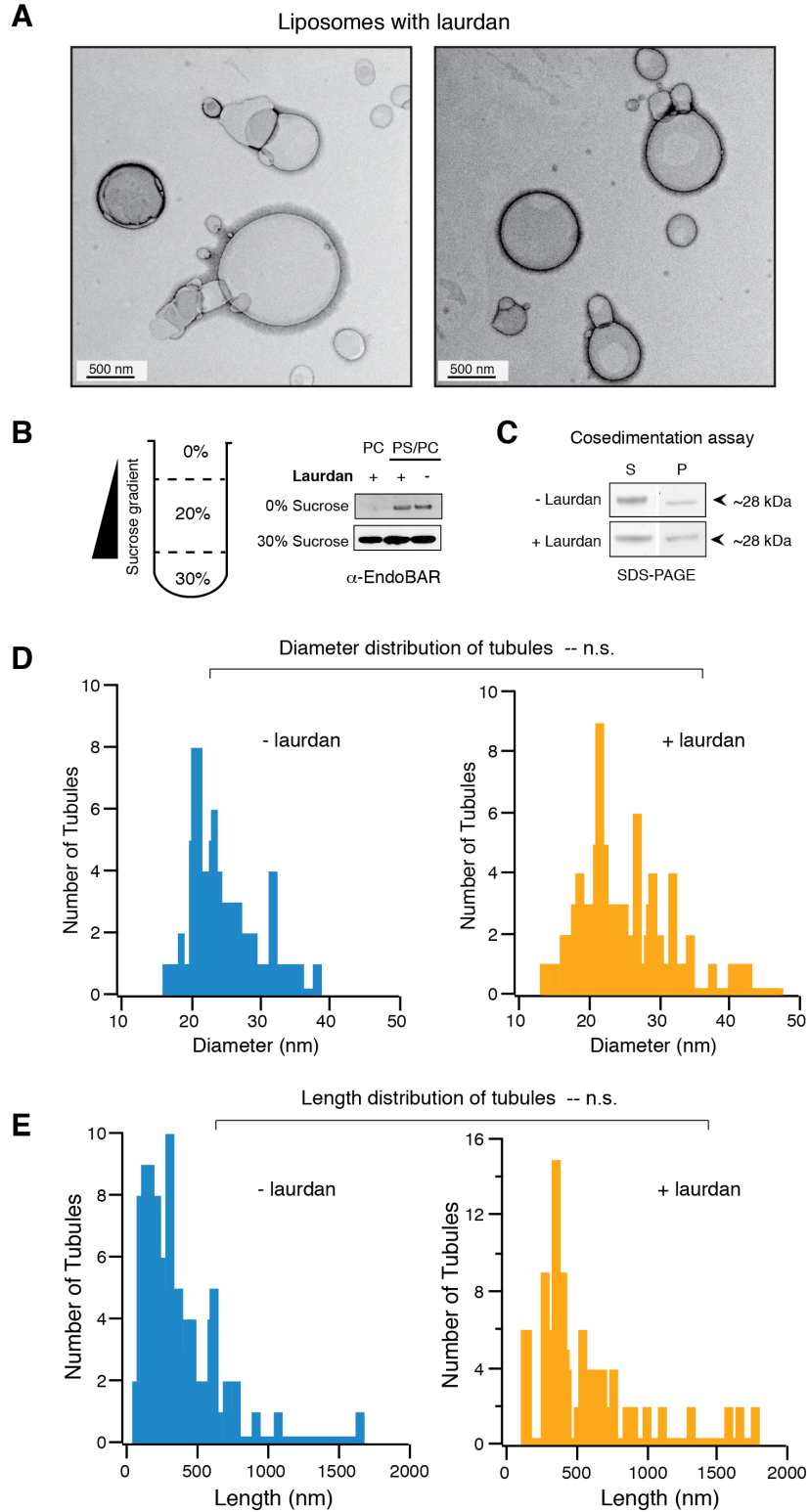
except that EndoFL was used to replace EndoBAR. Liposomes were prepared using extrusion

through polycarbonate filters with 1 μm pore sizes. The donor fluorophore Pacific Blue was

covalently linked to the native Cys residues (107,294,295). Rate constant k_{obs} is plotted as

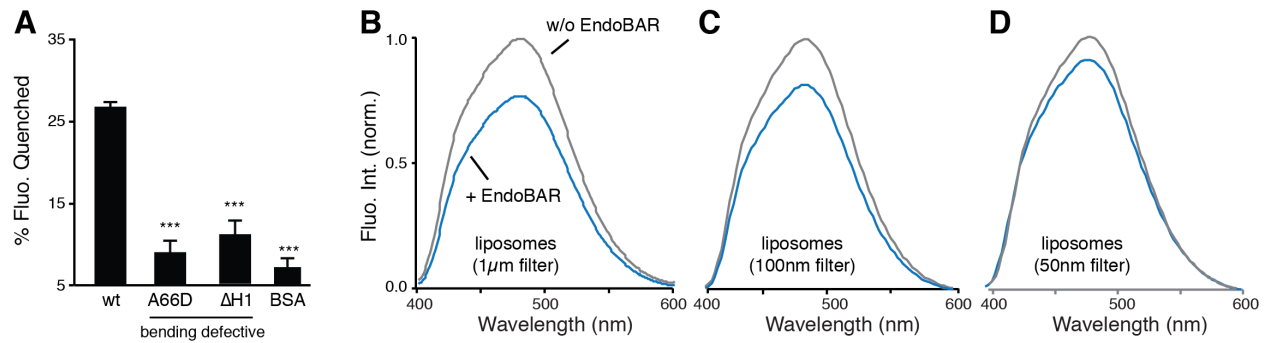
mean \pm standard deviation from 3 independent experiments. Experiments were repeated in

three independent trials.



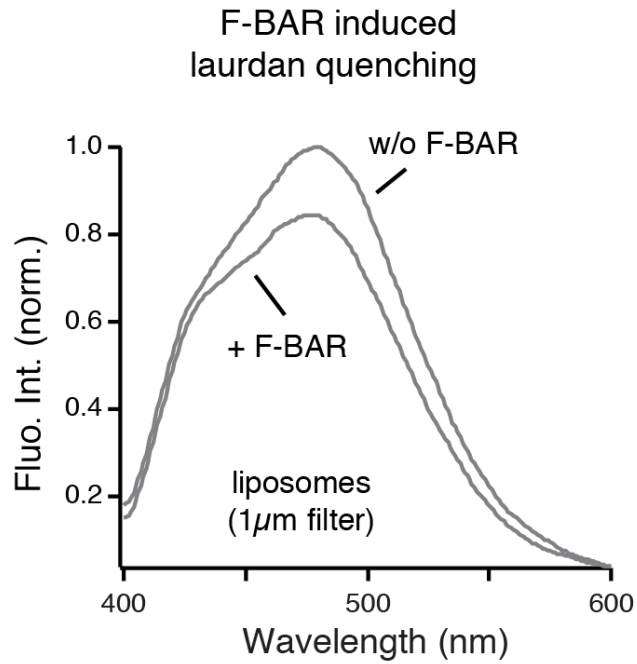
Supplementary Figure 4. Liposome morphology and Endo-BAR membrane interactions are not impaired by trace amounts of lauridan. Liposomes (25%PS, 70%PC, and 5%DPPE)

with (+) and without (-) a trace amount of laurdan (0.25%) were used in these studies. (A) Negative staining electron microscopy images show that liposomes harboring 0.25% laurdan have normal morphology. Sucrose gradient flotation assay (B) and cosedimentation assay (C) show that laurdan (0.25%) does not impair EndoBAR-membrane association. Liposomes that lack PS were used for control in the flotation assay. Western blots and coomassie blue stained SDS-PAGE gels are shown in panels B and C, respectively. Mouse monoclonal antibody against endophilin (Abcam 55702) was used to detect EndoBAR in panel B. (D-E) EndoBAR-induced membrane tubule diameter (D) and length (E) are shown in histogram plots. Liposomes with and without laurdan (0.25%) were used for comparison. Negative-staining TEM was used to visualize membrane tubules as described in methods. K-S tests show that there is no significant difference between samples with and without laurdan. All experiments were repeated in three independent trials.



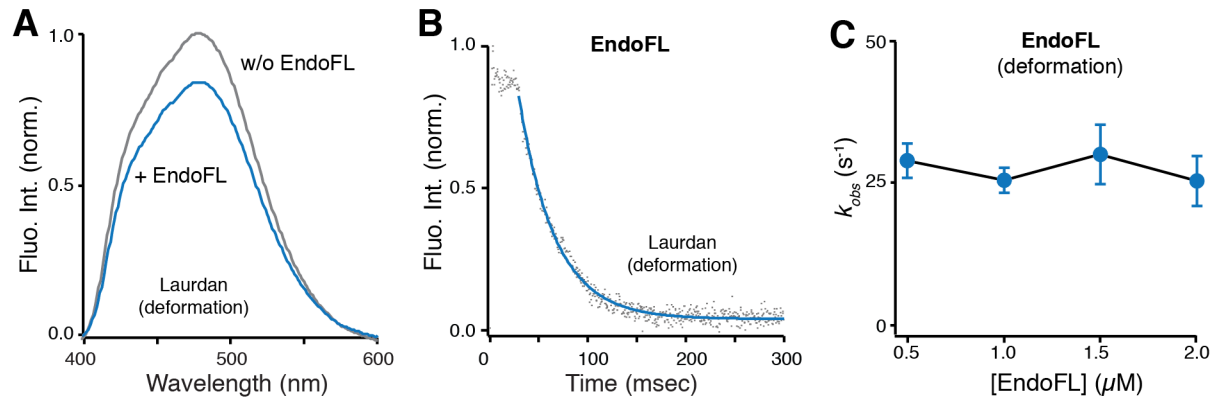
Supplementary Figure 5. Quenching of laurdan fluorescence relies on the bending

property of EndoBAR and liposome curvature. (A) Mutant versions (A66D and ΔH11) of EndoBAR that have defects in bending membranes in TEM analyses failed to induce laurdan quenching. BSA also failed to quench laurdan. Wild type and mutant EndoBAR (1 μM) were incubated with liposomes (prepared by 1 μm filters, 0.5 mM total lipids, 25%DOPS, 70%POPC, 5%DPPE, and 0.25% laurdan). *** indicates $p < 0.001$. Error bars indicate standard deviations. (B-D) The extent of laurdan quenching induced by EndoBAR depends on the initial diameter of liposomes. Liposomes prepared by extrusion through filters with 1 μm diameter pores (B), 100 nm pores (C), and 50 nm pores (D) were used. Lipid compositions in all liposomes were identical (0.5 mM total lipids, 25%DOPS, 70%POPC, 5%DPPE, and 0.25% laurdan). Laurdan was excited at 365nm. Experiments were repeated in three independent trials.



Supplementary Figure 6. The FCHO-1 F-BAR domain induces laurdan quenching.

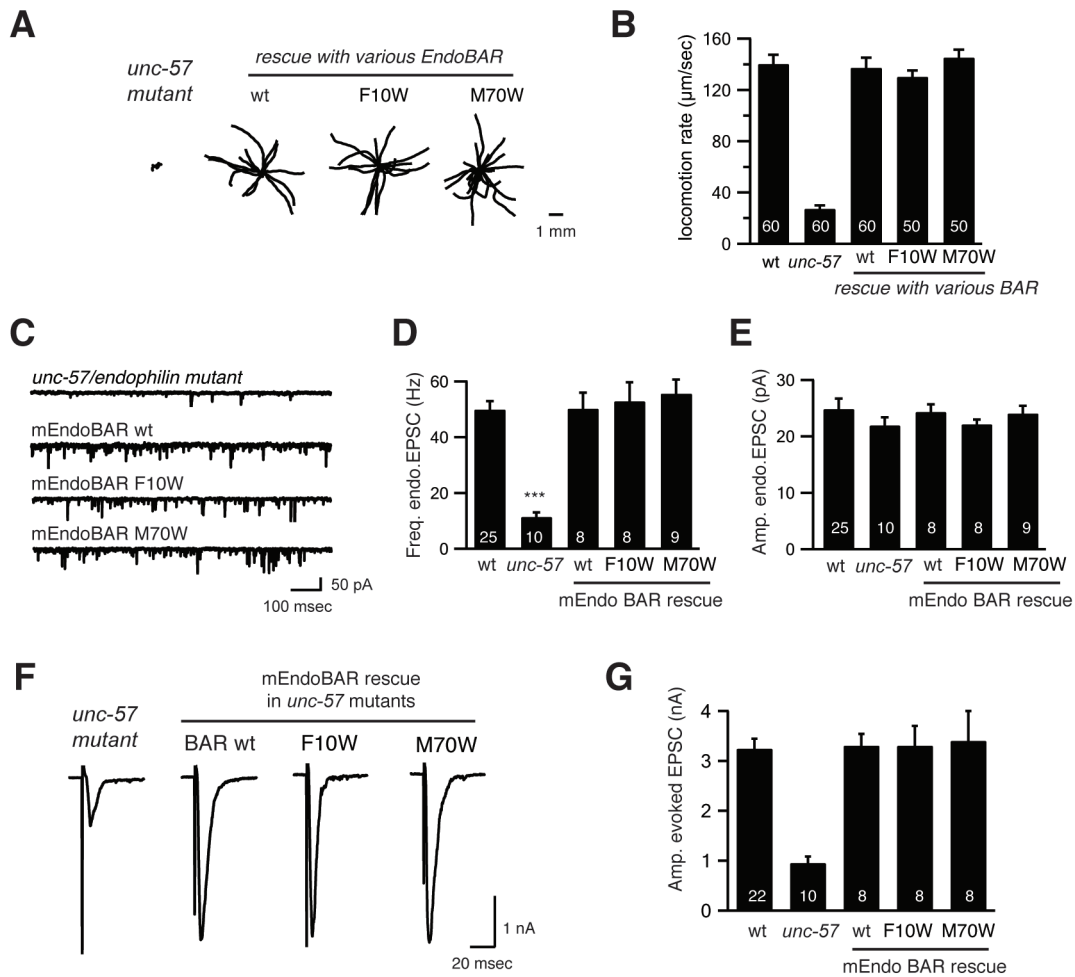
Liposomes (0.5 mM total lipids; 25%DOPS, 70%POPC, 5%DPPE, 0.25%laurdan) were incubated with the FCHO-1 F-BAR domain (1 μ M) for 10 minutes. Laurdan spectra were collected as described in the legend of Figure 2. Laurdan fluorescence intensity was significantly quenched by the F-BAR domain. Experiments were repeated in three independent trials.



Supplementary Figure 7. Full length endophilin deforms membranes with similar rates

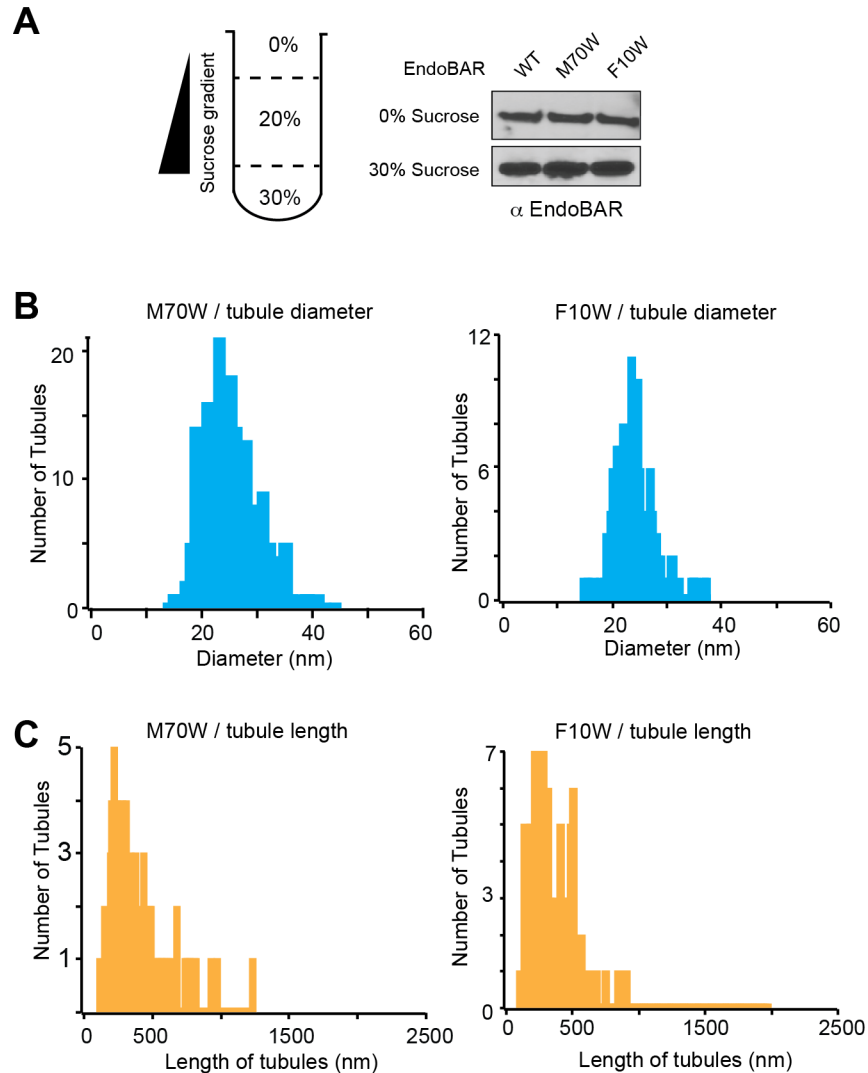
as the isolated BAR domain. The steady-state emission spectra (A) and the stopped-flow kinetic trace (B) using the laurdan assays reported that EndoFL deforms membranes.

Experiments were performed as described in the legend of Figure 2, except that EndoFL was used to replace EndoBAR. (C) The rate constants of laurdan quenching do not vary with the concentrations of EndoFL. Rate constant k_{obs} is plotted as mean \pm standard deviation from 3 independent experiments.



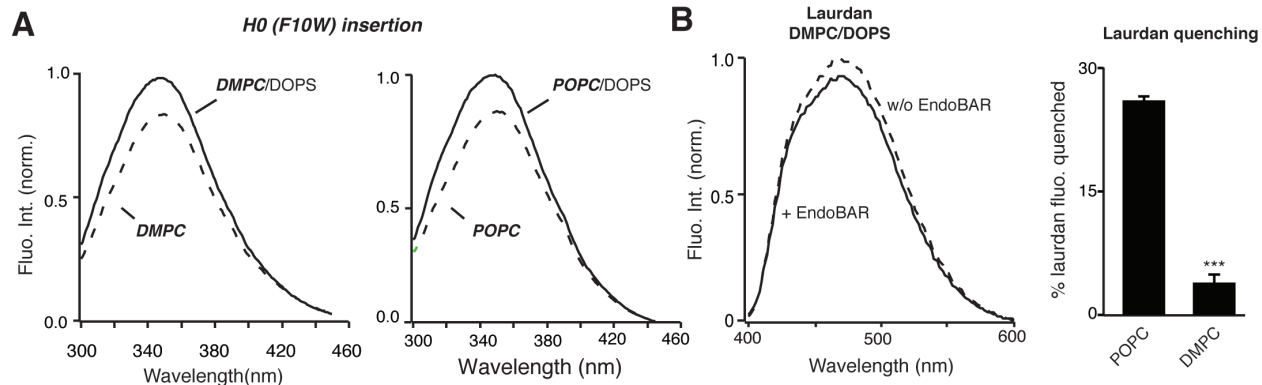
Supplementary Figure 8. F10W and M70W versions of EndoBAR are fully functional *in vivo*. A pan-neuronal promoter *Prab-3* was used to drive transgene expression. Transgenes encoding mouse EndoBAR variants were introduced into *unc-57(e406)* mutant worms by microinjection. (A-B) *C. elegans* locomotion is fully restored by neuronal expression of wild type (wt), F10W, or M70W versions of mEndoBAR. Representative trajectories (15 animals) of 30 secs locomotion are shown for each genotype. The starting points for each trajectory are aligned for clarity. Speed of locomotion is quantified in the panel (B). (C-G) Electrophysiological recordings show that F10W and M70W mutations do not impair EndoBAR's ability in supporting synaptic activity. Representative traces (C, F) and summary data for endogenous EPSC (excitatory postsynaptic currents) rates (D) and amplitudes (E), and for evoked EPSC

amplitudes (G) are shown for the indicated genotypes. The number of worms analyzed for each genotype is indicated in the bar graphs. Error bars represent standard error of the mean.



Supplementary Figure 9. Tryptophan mutations do not alter EndoBAR-membrane interactions *in vitro*. (A) A scheme for sucrose gradient flotation assay is shown at the *left* panel. The abundance of wild type, F10W, and M70W versions of EndoBAR in the top (0% sucrose) and bottom (30% sucrose) are quantified using western blots (*right* panels). EndoBAR is detected by a monoclonal antibody against endophilin (Abcam 55702), and is visualized by enhanced chemiluminescence. (B) Histogram analyses of the diameter of membrane tubules generated by F10W (*left*) and M70W (*right*) EndoBAR. (C) Histogram analyses of the length of membrane tubules generated by F10W (*left*) and M70W (*right*) EndoBAR. Experiments in (B-C) are carried out as described in the legend of Figure 7. K-S tests were applied to compare the

histogram plots generated by wild type (Supplemental Figure 4D-E) and Trp mutant EndoBAR.
No significant difference was detected.



Supplementary Figure 10. Helix insertion into rigid membranes does not induce laurdan

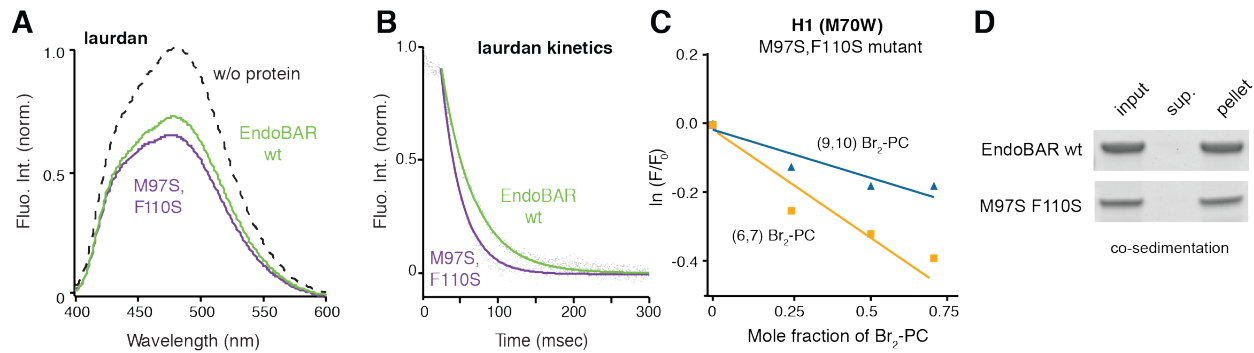
quenching. (A) DMPC does not impair H0 insertion into membranes. *Left panel:* Trp

fluorescence of EndoBAR F10W was used to monitor membrane insertion. Liposomes used in these experiments are the following: DMPC (95% DMPC and 5% DPPE; dashed line) and DMPC/DOPS (70% DMPC, 5% DPPE, and 25% DOPS; solid line) in the left panel; DOPC (95% DOPC and 5% DPPE; dashed line), and DOPC/DOPS (70% DOPC, 5% DPPE, and 25%

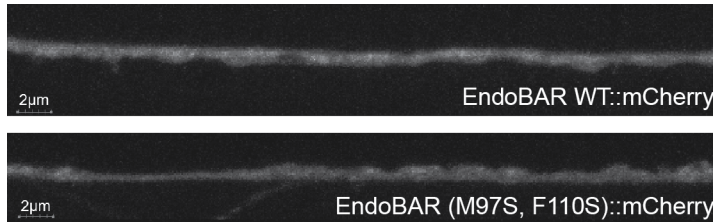
DOPS; solid line) in the right panel. (B) DMPC disrupts EndoBAR induced laurdan quenching.

Traces of laurdan fluorescence in the absence and presence of EndoBAR (1 μ M) are shown in the left panel. Percentage of laurdan quenching is plotted in the right panel. Liposomes used in all experiments were prepared using extrusion through polycarbonate filters with 1 μ m pore size.

Average data from three independent experiments were plotted in panel D. Error bars indicate standard deviation.



Supplementary Figure 11. Endophilin mutant with compromised helix insertion exhibits enhanced ability of local membrane deformation. The mutant (M97S, F110S) EndoBAR increases the extent of laurdan quenching (A), and accelerates the speed of membrane deformation (B). Depth analysis shows that the H1 helix of the mutant (M97S, F110S) EndoBAR does not penetrate deeply into the membranes (C). Co-sedimentation assays indicate that M97S, F110S mutant binds 50nm liposomes to a similar extent as the wild type EndoBAR (D). In all experiments, mutant EndoBAR was 1 μ M, and liposomes were prepared using filters with 1 μ m pores (except for co-sedimentation assays). Laurdan experiments were performed as described in the legend of Figure 2. The depth measurements were done as described in the legend of Figure 3 and the methods.



Supplementary Figure 12. Wild type and mutant EndoBAR have an identical localization pattern. Representative images of mCherry tagged wild type and mutant (M97S, F110S) versions of EndoBAR show that these proteins have similar distribution pattern in the dorsal nerve cord. Scale bars indicate 2µm. Images were collected on an inverted Olympus FV-1000 confocal microscope with an Olympus PlanApo 60x Oil 1.4 NA objective at 5x zoom.